A Cellular Positioning System to Probe Morphological Heterogeneity Among Mouse CA3 Hippocampal Pyramidal Neurons

Christopher J. Handwerk[a], Katherine M. Bland[a], Cooper A. Brett[a], Collin J. Denzler[a], Anna R. Kalinowski[a], Brian D. Swinehart[a], Hilda V. Rodriguez[a], Hollyn N. Cook[a], George S. Vidal[a]*
[a]*Department of Biology, James Madison University, MSC 7801, Harrisonburg, Virginia 22807, United States of America *To whom correspondence should be addressed. Email:* vidalgx@jmu.edu

Highlights

- We devised a method to probe morphological heterogeneity in CA3 pyramidal neurons.
- Our method uses replicable techniques available to most laboratories.
- We discovered correlated topographic/morphological variables among CA3 neurons.

Abstract

Background: Pyramidal neurons of the hippocampus are not homogeneous in their structure or function, yet the structure and function of individual neurons are well-correlated. Despite these well-known facts, few structural studies of pyramidal neuronal dendrites in the hippocampus have controlled for precise cellular position within the hippocampus along its dorsoventral (longitudinal), tangential (proximodistal), or radial axes. We believe this is largely due to technical limitations that limit positional information about the neuron, limit throughput, and limit the control of confounding variables.

New method: Here, we present a simple approach to address these limitations effectively in mouse CA3, adapted from our prior work in the mouse cerebral cortex. Our approach tracks the dorsoventral, tangential, and radial positions of neurons within the hippocampus, increases the number of available neurons for analysis, and provides several new controls.

Results: We demonstrate how topographic and morphological data are related to one another among mouse CA3 pyramidal neurons, in a pilot data set providing proof-of-concept.

Comparison with existing methods: Other common methods of labeling neurons, such as biocytin fills or Golgi-Cox stains, are labor- or time-intensive. Here, we validate the use of the transgenic fluorescent *Thy1*-GFP-M line, so the labeling step is practically eliminated. Other methods section the hippocampus coronally, which distorts the dorsoventral, tangential, and radial axes. Here, we preserve all three axes. Some existing methods do not collect all sections in order, instead focusing on “more dorsal” or “more ventral” sections, for example. We preserve much more dorsoventral information. Recent work has shown that CA2 is better defined by immunohistochemical rather than neuroanatomical markers. We use that immunohistochemistry here to increase precision in defining tangential position. Other studies have not measured other, critical variables and relationships that could confound the results. Here, we assess many more of these variables and relationships to increase the rigor of our work.

Conclusions: We developed a more rigorous method for preserving precise cellular positioning information among reconstructed mouse hippocampal pyramidal neurons. Although we provide several innovations in our method, each innovation identified here could independently improve the rigor and reproducibility of a wide variety of approaches for understanding the morphological heterogeneity of pyramidal neurons in the brain.

Keywords

CA3; pyramidal neuron; dendritic morphology; dendritic complexity; reconstruction; GFP-M

1 Introduction

Hippocampal pyramidal neurons are heterogeneous in their gene expression, structure, and function[1–4]. Some heterogeneous structural and functional features of these neurons vary in a topographically patterned way and are essential for proper hippocampal function. For example, in CA3, place field size, pattern completion, and sharp wave initiation are all arranged topographically[3,5–9]. Specific locations within CA3 are recruited during both spatial[10–14] and non-spatial learning and memory[15]. Focal lesions within specific CA3 subfields can lead to disrupted fear memory[16] or spatial processing[17]. Chronic social stress also perturbs CA3 dendritic morphology and concomitantly impairs spatial learning and memory, likely in a topographically patterned way[18].

The *stratum pyramidale* of CA3*,* home to CA3 pyramidal neuron somata, can be thought of as a sheet that extends along a tangential axis (*i.e.*, where neurons are more proximal or distal to the dentate gyrus) and along a dorsoventral, or “long”, axis (*i.e.*, where neurons are closer or further away from the septum). The *stratum pyramidale* also possesses a radial axis (*i.e.*, where neurons are deep or superficial within the *stratum pyramidale*). Despite the known heterogeneity in CA3, only a few studies have studied dendritic morphological variation systematically along any of the three axes[14,19,20]. Of these studies, one analyzed both the radial and tangential axes[19], and another studied the tangential and dorsoventral axes[20]. No study to date (to our knowledge) has studied dendritic morphology along all three axes simultaneously. We believe this is due to a methodological gap.

We sought to fill this gap by establishing proof of principle in collecting and analyzing detailed topographic and morphological variables of CA3 pyramidal neurons across all three axes. In designing our new method, we sought to rely on relatively simple laboratory techniques to increase its reproducibility and access by other laboratories. Our prior work used serial sections and sparsely labeled, green fluorescent protein (GFP)-filled neurons to discover a gradient of dendritic morphology across layer 2/3 of the mouse cerebral cortex[21], which is perturbed by the deletion of integrin β3 (*Itgb3*), an identified autism risk gene[22]. Here, we applied the same simple serial sectioning strategy, this time pairing it with the widely available and characterized *Thy1*-GFP-M line[23] as a relatively easy way to fill sparse subsets of CA3 pyramidal neurons with GFP.

2 Material and methods

An overview of the main methods is presented in Figure 1, and the details for each step are presented below.

2.1 Ethics statement

Our study complies with the ARRIVE 2.0 guidelines by including essential information regarding study design, sample size, inclusion/exclusion criteria, randomization, blinding, outcome measures, statistical methods, experimental animals, experimental procedures, and results, where applicable. The James Madison University Institutional Animal Care and Use Committee approved the necessary work with mice (protocol #20-1067). We followed the guidelines of the National Research Council’s Guide for the Care and Use of Laboratory Animals.

2.2 Mice

In our mouse colony, the Thy-1-GFP-M transgenic mouse[23] (STOCK Tg(Thy1-EGFP)MJrs/J, The Jackson Laboratory #007788) had been backcrossed to the C57BL6/J strain (The Jackson Laboratory #000664) for at least 5 generations by the time we bred mice for this study. A male transgenic (*i.e.*, hemizygous) *Thy-1*-GFP-M

mouse was bred with a female C57BL6/J mouse. To minimize the possibility that the sparse GFP patterning could be affected by genomic imprinting, we suggest selecting one sex consistently (in this case, males) as the *Thy-1*-GFP-M transgene carrier in any breeding strategy for experimentation. Approximately half of the progeny from this cross carried the transgene, as determined by genotyping of tissue acquired via ear punch (Transnetyx; probe “Thy1-3 Tg”). We selected one hemizygous female mouse at postnatal day 30 to collect pilot data for this method.

After birth, mice in our colony are housed with their parents and littermates until weaning. Mice are weaned approximately between postnatal day 21 and 28. Upon weaning, mice are housed with their same-sex littermates. All mice are housed in a temperature- and humidity-controlled, specific-pathogen-free environment with a 12-h light/dark cycle. Mouse cages are supplied with Teklad ¼” corncob bedding, with food (Teklad 18% protein rodent diet) and water supplied *ad libitum*.

2.2 Histology

2.2.1 Perfusion and dissection

We euthanized the mouse by intraperitoneal injection of ketamine (240 mg/kg)-xylazine (48 mg/kg)-acepromazine (1.85 mg/kg). Then, we transcardially perfused 50 mL of ice-cold 1× phosphate-buffered saline (PBS; diluted from OmniPur® 10× PBS Liquid Concentrate, Sigma #6505, with Milli-Q distilled water), followed by 50 mL of ice-cold, freshly made 4% (wt/vol) paraformaldehyde (Sigma-Aldrich) in PBS, pH 7.4 (4% PFA). We dissected the head and post-fixed it in 4% PFA for approximately 24 h at 4 °C. We dissected the brain out of the skull using two #5SF forceps (Fine Science Tools #11252-00) and a micro spatula (Fine Science Tools #10091-12) and dissected away the meninges. We made a midsagittal cut with a razor blade to separate the hemispheres. Keeping the brain moist with 1× PBS, we scooped out subcortical structures from each hemisphere (for this study, the left hemisphere) with the micro spatula, leaving the cortex and hippocampus intact. After removing as much white matter as possible near the hippocampus proper, we used the micro spatula to loosen the hippocampus proper from the cortex, then used the forceps to severe the hippocampus proper from the cortex.

2.2.2 Straightening the hippocampus

We placed the hippocampus on the middle of a glass slide, with the dorsal and ventral ends pointing toward the top and bottom of the slide. At this point in the procedure, the hippocampus still exhibits a curvature along the dorsoventral axis, so we adapted prior procedures to straighten the axis[24,25]. We stacked 22 × 22 mm #1 coverslips to match the height of the hippocampus (approximately eight coverslips) and placed this stack to the left of the hippocampus. We stacked the same number of 22 × 22 mm #1 coverslips to the right of the hippocampus. Then, we gently pushed the two coverslip stacks together, straightening the hippocampus. We placed a second glass slide on top and held the entire configuration together by binding the

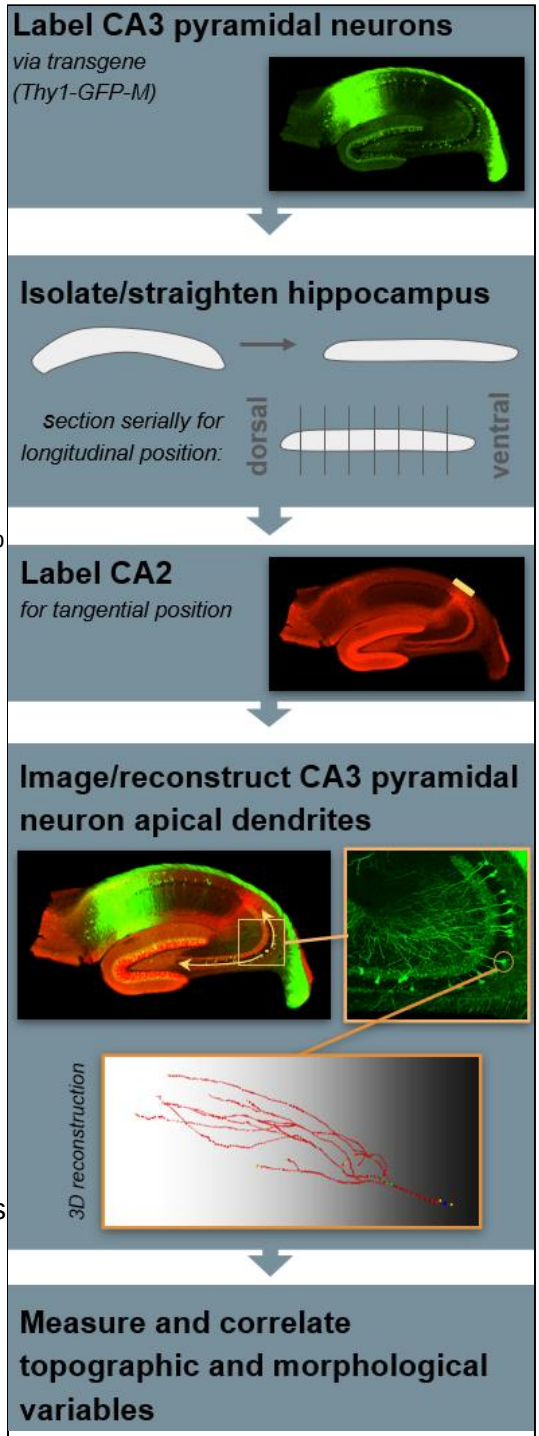

Figure 1. Schematic flowchart of methods. *[one-column figure]*

the glass slides together with mini binder clips. We immersed the entire configuration in a Petri dish with 1% PFA (wt/vol) diluted in 1× PBS, and incubated it overnight at 4 °C (an incubation time of 4 hours is sufficient to straighten the hippocampus).

2.2.3 Sectioning the hippocampus

We embedded the hippocampus in agar prior to sectioning. To do so, we first dissolved and melted 4% agar (wt/vol, in Milli-Q distilled water) on a hot plate. Off the heat, we stirred the agar as it cooled. Just before it hardened, we poured a 3-5 mm base of molten agar into a mold (2.5 mL glass micro beaker, Electron Microscopy Services #60982), laid the straightened hippocampus on top, and poured more molten agar on top of the hippocampus. Once the agar hardened, we blocked the agar on the platform of a vibrating microtome (Leica VT1000S), such that we could take 100 µm-thick free-floating transverse sections in 1× PBS. Critically, we collected each section in order on a 96-well, round-bottom micro plate that was pre-loaded with 1× PBS. We found that removing the agar around each free-floating section was not strictly necessary, but greatly aided in the pipetting that is required for subsequent immunohistochemistry (see below).

2.2.4 Immunohistochemistry

To enhance GFP fluorescence, we used the Mouse on Mouse (M.O.M.) Immunodetection Kit (Vector Laboratories, #BMK2202) in conjunction with mouse monoclonal anti-GFP (clone “3E6”, Invitrogen #A-11120), and goat anti-mouse IgG (H+L) $F(ab')_2$ fragment conjugated to Alexa Fluor 488 (Cell Signaling Technology, #4408). Each well, containing one section, received 50 µL of solution at each step. We followed the manufacturer’s instructions for preparing blocking solution and diluent. We incubated the tissue in blocking solution for 1 h, washed twice in 1× PBS, incubated in diluent for 5 minutes, incubated in primary antibody (1:1000 in diluent) for 30’, rinsed twice in 1× PBS, incubated in secondary antibody (1:250 in diluent), and rinsed thrice in in 1× PBS.

To stain for CA2 pyramidal neurons, we used rabbit polyclonal anti-PCP4 (Invitrogen #PA5-52209) and highly cross-adsorbed goat anti-rabbit IgG (H+L) conjugated to Alexa Fluor 594 (Invitrogen #A-11037). Each well, containing one section, received 50 µL of solution at each step. We incubated the tissue in blocking solution (5% [vol/vol] normal goat serum [Vector Laboratories #S-1000-20] and 0.15% [vol/vol] Triton X-100 [Sigma-Aldrich #T8787] in 1× PBS), incubated in primary antibody (1:1000 in blocking solution), rinsed twice in 1× PBS, incubated in secondary antibody (1:600 in blocking solution), and rinsed twice in 1× PBS.

2.2.5 Mounting and storing slides

We mounted sections directly on charged glass slides (Globe Scientific #1358L), applied ProLong Diamond Antifade Mountant (Invitrogen #P36970), and placed a #1 coverslip (Globe Scientific #1315-10) on top. We cured the slides for at least 48 h before imaging. For long-term storage, we have kept the slides at -20 °C.

2.3 Microscopy

2.3.1 Hippocampal sections

We took images of each hippocampal section to identify somata with GFP and/or PCP4 expression, using a Nikon Eclipse Ti-2 microscope with a 4× PlanApo objective (0.20 NA) in the “green” channel (excitation filter: 446-486 nm, emission filter: 500-550 nm, to capture GFP and Alexa Fluor 488 signal), and in “red” (excitation filter: 542-582 nm, emission filter: 604-678 nm, to capture Alexa Fluor 594 signal). We imaged 16 sections for this study.

2.3.2 CA3 pyramidal neurons

We took confocal z-stack images of GFP-positive, CA3 hippocampal pyramidal neurons, using a Nikon TE2000 C2si laser scanning confocal microscope with a 20× PlanApo objective (0.75 NA), exciting the GFP with a 488 nm laser. Neurons were chosen blind to their genotype or precise topographical position, though they were more likely to be selected if they were not next to other GFP-positive neurons. The density of GFP-positive neurons across the dorsoventral and tangential extent of CA3 appeared to be random, unlike CA1, where the density of GFP-positive cells clearly increases distally from the dentate gyrus. Within CA3, the likelihood that a particular neuron would be GFP-positive or negative also appeared to be random, which is why we were not concerned about selecting neurons that had minimal overlap with GFP-positive dendrites from other neurons. We also selected neurons that had intact apical arbors, which meant that their somata were generally found in the middle of the section thickness. When taking an image, we positioned the soma at one end of the field-of-view, such that the image captured the entire apical dendrite. The entire thickness of the section was imaged with a step size of 0.7 µm. We imaged a total of 17 neurons from 9 sections for this study. Based on this experience, we believe that 17 is an approximate upper limit to the number of neurons with sufficient quality for reconstruction using this method.

2.4 Analysis

2.4.1 Topographical positioning: Depth in *stratum pyramidale*, depth in section

The *stratum pyramidale* is distinguishable from the *stratum lucidum* and from the *stratum* oriens in the 20× confocal images we captured. We used Fiji software[26] to measure the radial distance between the neuron soma center and the center of the *stratum pyramidale*, with somata superficial to the center of the *stratum pyramidale* recorded as having negative values. We called this distance “depth in *stratum pyramidale*”. We also measured the distance along the z-axis from the top of the section (closest to the coverslip) to the neuron soma center as well as from the bottom of the section (closest to the glass slide) to the neuron soma center to calculate the relative depth of the soma within the section (with 0 meaning that it was adjacent to the coverslip, and 1 meaning that it was adjacent to the glass slide). We called this calculation “depth in section”.

2.4.2 Topographical positioning: DG length, DG width, CA2 length, CA3 length

The granule cell layer of the dentate gyrus is distinguishable in the 4× images we captured. We used FIJI software to measure the length of the granule cell layer, which we called “DG length”. We also measured the distance between the tip of the infrapyramidal blade of the granule cell layer and the tip of the suprapyramidal blade of the granule cell layer, which we called “DG width”.

PCP4 immunohistochemistry allows for the precise identification of CA2[27,28]. We used the procedure validated by San Antonio *et al.*[29] (Gaussian blur of 20 µm, 50% local maximal intensity) to determine the immunohistochemical border between CA2 and CA1, as well as between CA2 and CA3. In our case, we used Fiji rather than Adobe Photoshop, utilizing the “Gaussian blur” and “PlotProfile” functions. We then measured the distance (along the superficial border of the *stratum pyramidale*) between the two determined borders, which we called “CA2 length”. We also measured the distance along the *stratum pyramidale* from the border between CA2 and CA3 and the proximal end of the *stratum pyramidale* in CA3, which we called “CA3 length”.

2.4.3 Topographical positioning: Transverse distance from DG, transverse distance from CA2, relative transverse distance

Each cell captured at 20× was registered to the 4× image of its corresponding hippocampal section using Fiji software. We measured the distance (along the superficial border of the *stratum pyramidale*) from the proximal end of the *stratum pyramidale* to the neuron soma center, which we called “transverse distance from DG”. We also measured the distance (along the superficial border of the *stratum pyramidale*) from the border between CA2 and CA3 and the neuron soma center, which we called “transverse distance from CA2”. With these

measurements, we calculated the relative distance of the neuron along the *stratum pyramidale* of CA3 (with 0 meaning it is most distal from dentate gyrus, and with 1 meaning it is most proximal to dentate gyrus), which we called “relative transverse distance”. values between 0 to ⅓ correspond to CA3a (according to the nomenclature coined by Lorente De Nó[30]), values between ⅓ to ⅔ correspond to CA3b, and values between ⅔ to 1 correspond to CA3c.

2.4.4 Topographical positioning: Dorsoventral position

Because we took serial sections, we already knew the dorsoventral (also called “septotemporal”, “long”, or “longitudinal”) position of the neuron relative to the hippocampus analyzed. To record the dorsoventral position of the neuron relative to all hippocampal sections that could be developed with this method, we plotted the DG length, DG width, and CA3 length of each section, which can be predicted by their absolute dorsoventral position in both rats[24] and mice[20], regardless of sex or laterality. We assigned an arbitrary number (in this case, zero) to the middle section, and gave positive numbers to more dorsal sections that corresponded to their actual relative distance from the middle section. Sections from other hippocampi could be aligned to these sections by aligning their DG length, DG width, and CA3 length to this hippocampus. We called this measurement “dorsoventral position”.

2.4.5 Reconstruction and morphological measurements

We used neuTube software[31] to generate 3D semi-automated reconstructions from the 20× images we captured. These were saved as standard .swc reconstruction files, which we also inspected using the Simple Neurite Tracer plugin[32] in Fiji, ensuring that the soma and apical dendrites were categorized correctly by neuTube. Reconstructions will be made available on the NeuroMorpho.org repository[33,34]. We analyzed the .swc files using L-Measure software[35]. These morphological measurements are summarized in Table 1.

Table 1. Morphological measurements

Type	Name	Description	L-Measure: “Specificity”	L-Measure: “Function”	L-Measure: “Output”
Length	Total length	The sum of the total length of dendrites of all apical branch orders	n/a	n/a	n/a
Length	Euclidean length	The longest distance from the soma to the tip of an apical dendrite, measured “as the crow flies”	Type = 4 (apical dendrites)	EucDistance	Maximum
Length	Path length	The longest distance from the soma to the tip of an apical dendrite, measured along the dendrite	Type = 4	PathDistance	Maximum
Length	Primary length	The length of the primary apical dendrite	Type = 4; Branch_Order = 0	Length	Total_Sum
Length	Secondary length	The total length of the secondary apical dendrites	Type = 4; Branch_Order = 1	Length	Total_Sum
Length	Tertiary length	The total length of the tertiary apical dendrites	Type = 4; Branch_Order = 2	Length	Total_Sum
Length	Quaternary length	The total length of the quaternary apical dendrites	Type = 4; Branch_Order = 3	Length	Total_Sum
Length	Quinary length	The total length of the quinary apical dendrites	Type = 4; Branch_Order = 4	Length	Total_Sum
Length	Senary length	The total length of the senary apical dendrites	Type = 4; Branch_Order = 5	Length	Total_Sum
Length	Septenary length	The total length of the septenary apical dendrites	Type = 4; Branch_Order = 6	Length	Total_Sum
Diameter	Overall diameter	The average diameter of the entire apical dendrite	Type = 4	Diameter	Average
Diameter	Primary diameter	The average diameter of the primary apical dendrite	Type = 4; Branch_Order = 0	Diameter	Average
Diameter	Secondary diameter	The average diameter of the secondary apical dendrites	Type = 4; Branch_Order = 1	Diameter	Average
Diameter	Tertiary diameter	The average diameter of the tertiary apical dendrites	Type = 4; Branch_Order = 2	Diameter	Average
Diameter	Quaternary diameter	The average diameter of the quaternary apical dendrites	Type = 4; Branch_Order = 3	Diameter	Average

Diameter	Quinary diameter	The average diameter of the quinary apical dendrites	Type = 4; Branch_Order = 4	Diameter	Average
Diameter	Senary diameter	The average diameter of the senary apical dendrites	Type = 4; Branch_Order = 5	Diameter	Average
Diameter	Septenary diameter	The average diameter of the septenary apical dendrites	Type = 4; Branch_Order = 6	Diameter	Average
Branching	Total branch points	The total number of branch points on the entire apical dendrite	Type = 4	N_bifs	Total_Sum
Branching	Tertiary branches	The total number of branches that are tertiary dendrites	Type = 4; Branch_Order = 2	N_branch	Total_Sum
Branching	Quaternary branches	The total number of branches that are quaternary dendrites	Type = 4; Branch_Order = 3	N_branch	Total_Sum
Branching	Quinary branches	The total number of branches that are quinary dendrites	Type = 4; Branch_Order = 4	N_branch	Total_Sum
Branching	Senary branches	The total number of branches that are senary dendrites	Type = 4; Branch_Order = 5	N_branch	Total_Sum
Branching	Septenary branches	The total number of branches that are septenary dendrites	Type = 4; Branch_Order = 6	N_branch	Total_Sum

2.4.6 Statistics

We calculated two-tailed, 95% confidence-interval Pearson's correlation coefficients on all combinations of the 10 position variables to test if any variables had a linear relationship to one another. To control the false discovery rate (FDR) on these 45 correlations, we applied the method of Benjamini et al.[36] and set a 10% FDR threshold. We calculated 276 correlation coefficients on all combinations of the 24 morphological variables in the same way. Finally, to compare position variables against morphological variables, we again used the identical procedure to calculate 108 correlation coefficients. We used GraphPad Prism 9 software to calculate statistics and produce graphical representations of statistical calculations.

3 Results

3.1 GFP and PCP4 expression patterns

We observed that the overall pattern of GFP-positive somata in the hippocampus proper was restricted to the *stratum pyramidale* of the *cornu Ammonis* and to the granule cell layer of the dentate gyrus (Figure 1). GFP-positive somata were very densely packed in CA1, especially distal to the dentate gyrus, approaching the subiculum. Sparser expression was found in the granule cell layer of the dentate gyrus (Figure 1). The sparsest expression was found in proximal CA1, in CA2, and throughout CA3 (Figure 1). Bright, non-somatic GFP expression was found in the alveus and fimbria (Figure 1), likely representing efferents of GFP-positive somata in the hippocampus proper. Non-somatic expression was also found in the *stratum lucidum* of CA3 (Figure 1), likely representing efferent mossy fibers from dentate gyrus. In the *cornu Ammonis*, GFP-positive neurons had brightly labeled apical and basal dendrites, and in sparser regions, these could be distinguished from one another, particularly among apical dendrites.

We also observed strong somatic expression of PCP4 in the granule cell layer of the dentate gyrus and strong non-somatic PCP4 expression in the *stratum lucidum* of CA3 (Figure 1). PCP4 expression was also prevalent among CA2 somata, with strong expression extending into their apical and basal dendrites, hence there was also strong PCP4 expression in *stratum radiatum* and *stratum oriens* of CA2 (Figure 1).

3.2 Topographic data

We tested correlations among topographic data and found eight strong linear relationships ($p < 0.0191$, $r = 0.73$-0.98; Figure 2). Five of these correlations were between variables related to the dorsoventral axis (CA3 length, DG length, DG width, and dorsoventral position), and the other three were between variables related to the position of the neuron along the transverse axis (transverse distance from CA2, transverse distance from DG, and relative transverse distance; Figure 2). Figure 3 explores these linear relationships in detail. Moving from dorsal sections to ventral sections (*i.e.*, positive to negative dorsoventral position values), CA3 length generally increases (Figure 3A) and DG width generally increases (Figure 3B), but DG length generally decreases (Figure 3C). Thus, CA3 length and DG length are inversely correlated (Figure 3D), and DG length and DG width are inversely correlated (Figure 3E). Along the transverse axis, an expected relationship is present: the more distal a CA3 neuron is from DG, the closer it will generally be to the border with CA2 (Figure 3F). Relative transverse distance is thus correlated with one of these variables (transverse distance from CA2; Figure 3G) but negatively correlated with the other (transverse distance from DG; Figure 3H). Qualitatively, it is not apparent that there is any nonlinear component present in addition to the linear component in any of the eight correlations (Figure 3).

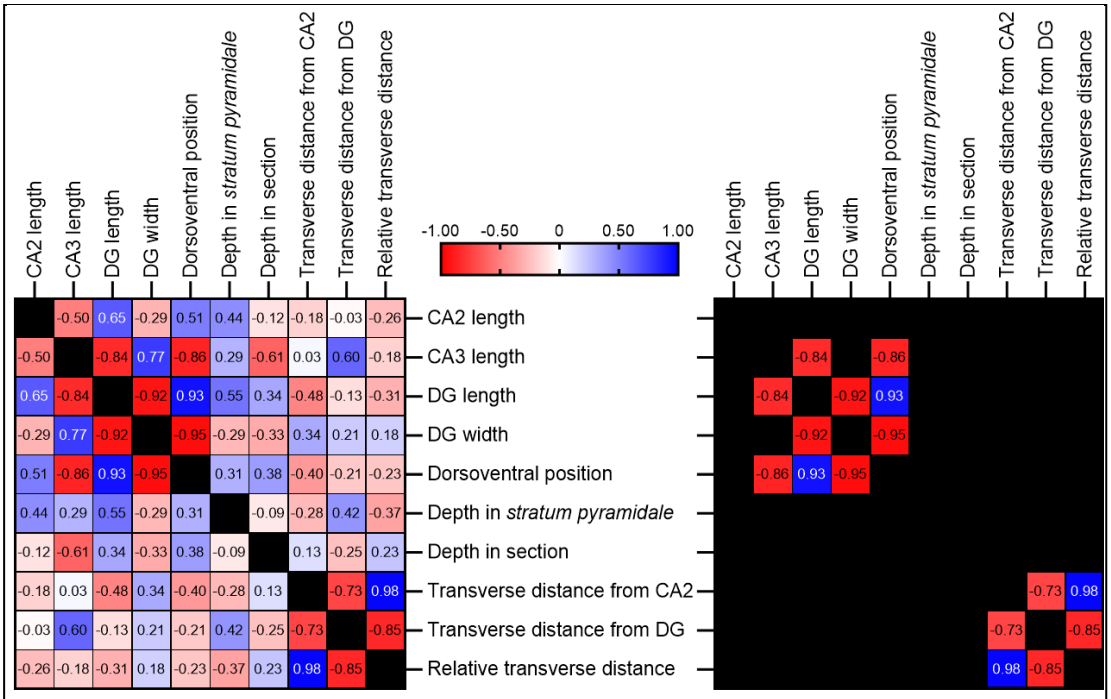

Figure 2. Pearson's correlation coefficients (r) of topographic variables. Left: All 45 correlations. Right: The 8 correlations under the 10% FDR threshold ($p < 0.0191$). *[1.5-column figure]*

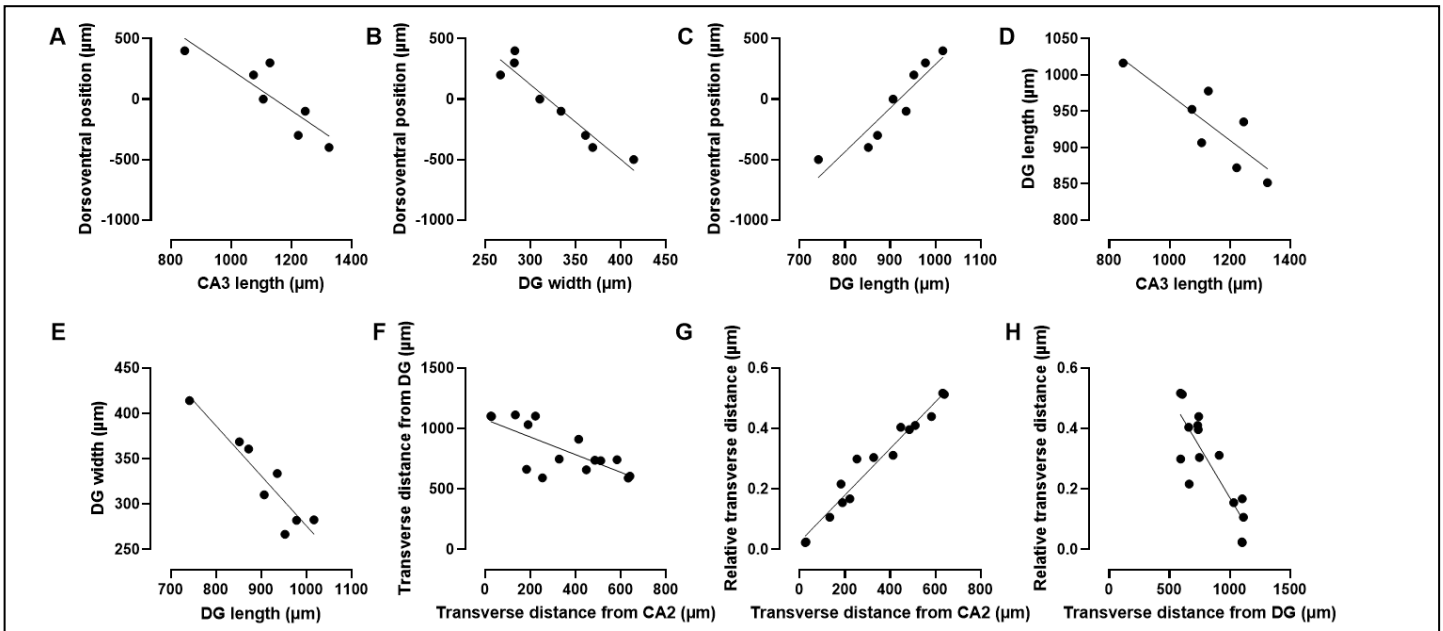

Figure 3. Eight topographic linear correlations identified in Figure 2 ($p < 0.0191$). *[2-column figure]*

3.3 Morphological data

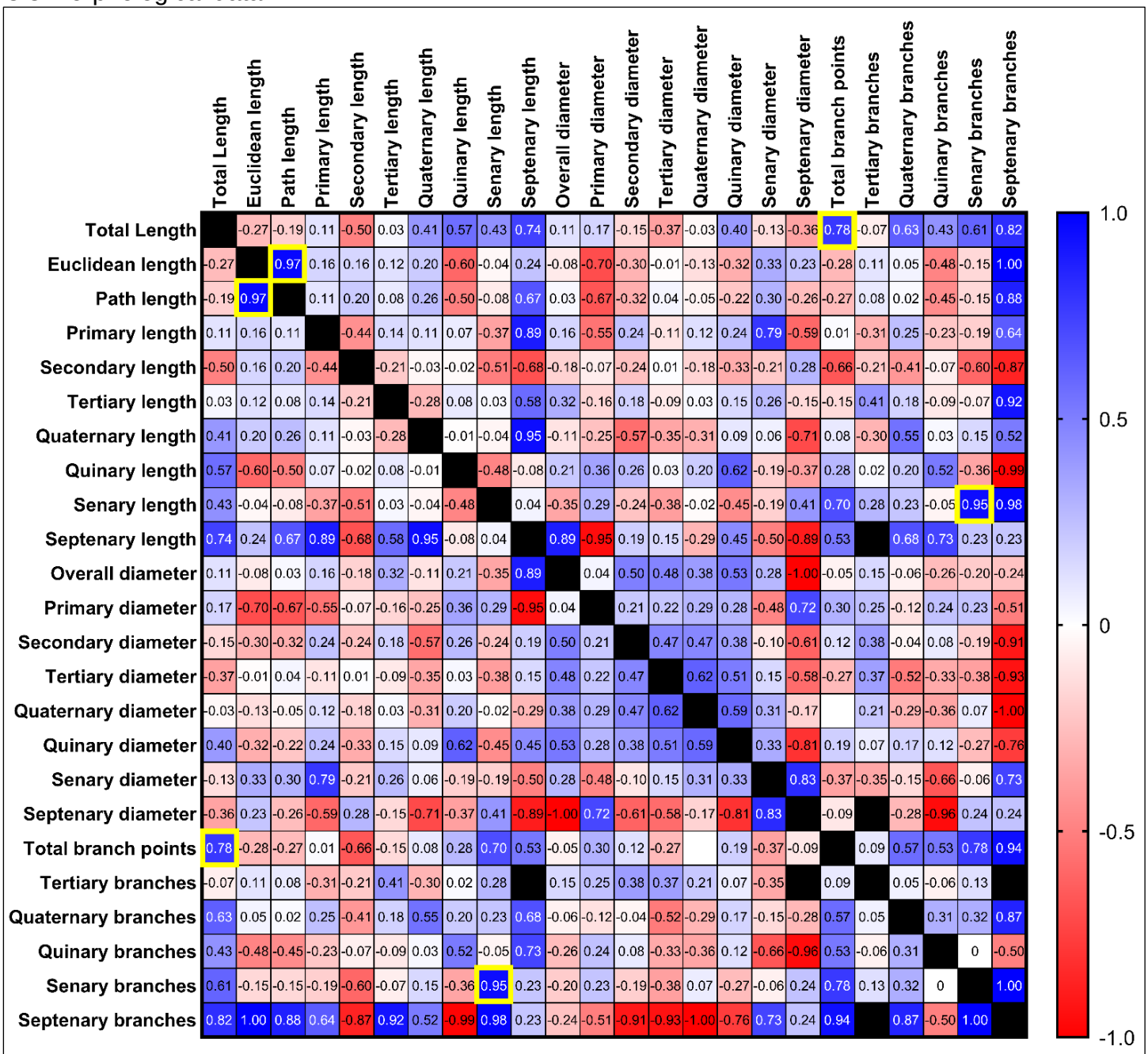

Figure 4. Pearson's correlation coefficients (r) of morphological variables. The three correlations under the 10% FDR threshold ($p < 0.0010$) are highlighted with a yellow box. *[two-column figure]*

Figure 4 shows the Pearson's r for all possible pairs of morphological variables. When testing for correlations among morphological data, we found three strong linear relationships ($p < 0.0010$, $r = 0.78$-0.97; Figure 4). One of the three relationships (senary branches *versus* senary length) had a single univariate outlier that violated the assumptions for Pearson's r, so this relationship was invalidated. The other two relationships are shown in Figure 5. First, we found that neurons with more apical branch points generally had a greater total apical length. Second, we found that the path length (which takes the tortuosity of the apical dendrite into account) and the Euclidean length of the dendrite (which does not take tortuosity into account) are positively correlated. As with the topographic variables, there is no apparent nonlinear component in these two correlations (Figure 5). We also noticed (Figure 4) that total length better correlated to the length of higher branch orders (quaternary and higher), that the diameter of most branch orders may be positively correlated to one another, and that the primary dendrite diameter may be correlated with shorter primary dendrites and a

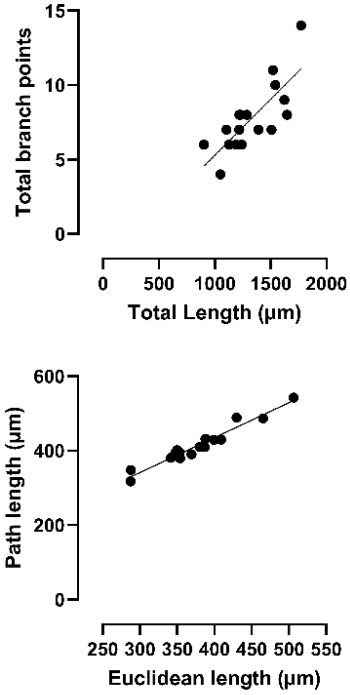

Figure 5. Two morphological linear correlations ($p < 0.0010$) identified in Figure 4. *[1-column figure]*

shorter Euclidean/path length, although these relationships are not conclusive because they were above the 10% FDR threshold. Similarly, we also tested for correlations between pairs of topographic and morphological variables (data not shown), but we did not find any conclusive linear relationships (*i.e.*, under the FDR threshold of 10%).

4 Discussion

We developed a method that records the detailed position of a neuron (with 10 topological variables) as well as its detailed morphology (with 24 morphological variables). Use of the *Thy1*-GFP-M line in conjunction with serial sectioning is a simple transgenic strategy that permits the full reconstruction of apical dendrites of CA3 pyramidal neurons. This method of labeling neurons for reconstruction is much less time-consuming and much more consistent when compared to other, commonly employed methods, such as neurobiotin/biocytin fills (taking several hours, dependent on the health of the section during the fill, and being low-throughput), or Golgi-Cox staining (which is higher throughput, takes days to weeks, and has tissue-to-tissue variability in the signal-to-noise ratio). In our experience, the slowest step of our method is in 3D reconstruction, which is semi-automated. We have not had success with fully automated, unsupervised reconstruction methods yet. Another positive feature of this method is that straightening the hippocampus to section the hippocampus exactly perpendicular to its dorsoventral axis ensures minimal distortion among all three topographic axes.

We suggest that several variations of this method could be used successfully by other investigators, depending on the experimental need. For example, if only information about the radial and dorsoventral axes were needed, the PCP4 stain could be eliminated entirely. Additionally, the *Thy1*-GFP-M line labels the mossy fibers of the dentate gyrus as they travel through the *stratum lucidum* of CA3 (Figure 1), so it may even be possible to determine the tangential extent of CA3 in this way as an alternative to the PCP4 stain. We also posit that it may be possible to eliminate the anti-GFP stain. In working with the *Thy1*-GFP-M line, we have noticed that endogenous GFP-M expression is high if the fixation time is not extended and ProLong Diamond mountant is used, but we have not tested this observation further. We also suggest that this method could be compatible with methods such as patch clamp electrophysiology if serial sections are tracked carefully throughout the procedure. However, the investigator would need to accept the inevitable distortion of the topographic axes by omitting the straightening step, which may require hours in fixative to achieve. We also surmise that it may be possible to include CA2 and even CA1 in these analyses, but each region would have its own difficulties that are not present in CA3. For example, in CA2, this method would likely yield a very low total number of reconstructed neurons per hippocampus due to the relatively small size of the field (Figure 1). In CA1, the density of GFP-positive neurons increases distally from the dentate gyrus (Figure 1), and a higher density of labeled neurons may make reconstruction difficult or altogether impossible. Thus, studies utilizing this method in CA1 would likely need to take selection bias along the tangential axis into account.

Among topographic variables, the relationships we found along the dorsoventral axis among DG length, DG width, and CA3 length are in line with other studies[20,24]. The fact that DG length increases and DG width decreases as one moves dorsally is in line with the qualitative observation that the dentate gyrus appears to have a wider “U” shape more ventrally and a narrower “V” shape more dorsally[24]. Among morphological variables, the fact that the Euclidean and path length of the apical dendrite were similar suggests that CA3 apical dendrites have little tortuosity. Finally, we observed that the strongly correlated topographical and

morphological variables did not appear to have any additional nonlinear relationships, making it unlikely that there is a discrete or abrupt change in these variables within CA3.

Of course, several limitations apply to this method. For example, our statistical analysis was restricted to testing linear relationships between pairs of variables. Although the linear relationships identified did not appear to have an additional nonlinear component, this observation clearly cannot be extended to the other pairs of variables that were not presented in Figure 3 or Figure 5. Because of this, we cannot exclude the possibility that additional variable pairs are related in some nonlinear way. Another limitation was that 17 neurons seemed to be an upper limit to the number of CA3 neurons that could be analyzed per hippocampus. Although this sample size seems small, it does have 80% power to detect an r^2 of 0.40 or higher. Our pilot study also cannot provide information about how much topographic or morphological variables might vary between one hippocampus and the next—in other words, we do not know if topographic or morphological data are clustered by hippocampus in some way. In a larger study including multiple hippocampi, investigators must be careful to account for any potential clustering in the data that would reduce the effective sample size[37]. Another limitation is that we did not reconstruct the basal dendrites of CA3 pyramidal neurons. This was because basal dendrites extended much more in the dorsoventral and tangential axes than the apical dendrites, so it was difficult to distinguish basal dendrites belonging to different neurons reliably. An alternative approach would be to adapt this method with another transgenic line or even an altogether different labeling strategy. Finally, another potential limitation is that our section thickness (100 µm) was too thin to accurately reconstruct apical dendrites, but we should have seen an obvious effect of “depth in section” on the morphology of the neuron if this were a significant problem. In this method, choosing the section thickness is actually a balance between achieving higher resolution of dorsoventral topographic information (by taking thinner sections) and higher resolution of the overall dendritic morphology (by taking thicker sections), so the optimal thickness will depend on the study objectives.

4.1 Conclusion

Increasing access to detailed topographic and morphological information is an important objective for eliminating confounds and increasing rigor and reproducibility in morphological studies of hippocampal pyramidal neurons. This objective is especially important when assessing behavioral/environmental perturbations (such as chronic social stress) or gene mutations that may affect the morphology CA3 pyramidal neurons in a topographically or morphologically selective manner. Adopting some or all of the methods presented here should assist neuroscientists in achieving this objective.

Declaration of interest

Declarations of interest: none.

Contributors

CH: conceptualization, data curation, formal analysis, investigation, methodology, project administration, supervision, validation, visualization, writing - original draft, writing - review & editing. KB: conceptualization, investigation, methodology, project administration, supervision. CB, CD, AK, BS, HR, HC: investigation, methodology. GV: conceptualization, data curation, formal analysis, funding acquisition, investigation, methodology, project administration, resources, supervision, validation, visualization, writing - original draft, writing - review & editing.

Funding

This work was supported by the National Institute for Neurological Disorders and Stroke of the National Institutes of Health (grant K01NS107723). No funding body influenced the experimental design, experimentation, or interpretation in this report, or the decision to submit the report for publication.

Acknowledgements

We are very grateful to Mses. Stephanie Atkins and Sarah Keegan for their superlative animal care.

References

1. Thompson CL, Pathak SD, Jeromin A, Ng LL, MacPherson CR, Mortrud MT, Cusick A, Riley ZL, Sunkin SM, Bernard A, Puchalski RB, Gage FH, Jones AR, Bajic VB, Hawrylycz MJ, Lein ES. Genomic Anatomy of the Hippocampus. Neuron. 2008 Dec;60(6):1010–1021.

2. Dong HW, Swanson LW, Chen L, Fanselow MS, Toga AW. Genomic–anatomic evidence for distinct functional domains in hippocampal field CA1. Proc Natl Acad Sci. Proceedings of the National Academy of Sciences; 2009 Jul 14;106(28):11794–11799.

3. Oliva A, Fernández-Ruiz A, Buzsáki G, Berényi A. Spatial coding and physiological properties of hippocampal neurons in the Cornu Ammonis subregions: SPATIAL CODING AND PHYSIOLOGICAL PROPERTIES OF HIPPOCAMPAL NEURONS. Hippocampus. 2016 Dec;26(12):1593–1607.

4. Cembrowski MS, Spruston N. Heterogeneity within classical cell types is the rule: lessons from hippocampal pyramidal neurons. Nat Rev Neurosci. 2019 Apr;20(4):193–204.

5. Kjelstrup KB, Solstad T, Brun VH, Hafting T, Leutgeb S, Witter MP, Moser EI, Moser MB. Finite Scale of Spatial Representation in the Hippocampus. Science. American Association for the Advancement of Science; 2008 Jul 4;321(5885):140–143.

6. Komorowski RW, Garcia CG, Wilson A, Hattori S, Howard MW, Eichenbaum H. Ventral Hippocampal Neurons Are Shaped by Experience to Represent Behaviorally Relevant Contexts. J Neurosci. Society for Neuroscience; 2013 May 1;33(18):8079–8087. PMID: 23637197

7. Masukawa LM, Benardo LS, Prince DA. Variations in electrophysiological properties of hippocampal neurons in different subfields. Brain Res. 1982 Jun 24;242(2):341–344. PMID: 7116139

8. Lu L, Igarashi KM, Witter MP, Moser EI, Moser MB. Topography of Place Maps along the CA3-to-CA2 Axis of the Hippocampus. Neuron. 2015 Sep 2;87(5):1078–1092. PMID: 26298277

9. Lee H, Wang C, Deshmukh SS, Knierim JJ. Neural Population Evidence of Functional Heterogeneity along the CA3 Transverse Axis: Pattern Completion versus Pattern Separation. Neuron. 2015 Sep;87(5):1093–1105.

10. Chawla MK, Sutherland VL, Olson K, McNaughton BL, Barnes CA. Behavior-driven arc expression is reduced in all ventral hippocampal subfields compared to CA1, CA3, and dentate gyrus in rat dorsal hippocampus. Hippocampus. 2018 Feb;28(2):178–185. PMCID: PMC5777901

11. Beer Z, Chwiesko C, Sauvage MM. Processing of spatial and non-spatial information reveals functional homogeneity along the dorso-ventral axis of CA3, but not CA1. Neurobiol Learn Mem. 2014 May;111:56–64. PMID: 24657342

12. Flasbeck V, Atucha E, Nakamura NH, Yoshida M, Sauvage MM. Spatial information is preferentially processed by the distal part of CA3: implication for memory retrieval. Behav Brain Res. 2018 Jul

16;347:116–123. PMID: 29518437

13. Beer Z, Vavra P, Atucha E, Rentzing K, Heinze HJ, Sauvage MM. The memory for time and space differentially engages the proximal and distal parts of the hippocampal subfields CA1 and CA3. PLoS Biol. 2018 Aug;16(8):e2006100. PMCID: PMC6136809

14. Sun Q, Sotayo A, Cazzulino AS, Snyder AM, Denny CA, Siegelbaum SA. Proximodistal Heterogeneity of Hippocampal CA3 Pyramidal Neuron Intrinsic Properties, Connectivity, and Reactivation during Memory Recall. Neuron. Elsevier; 2017 Aug 2;95(3):656-672.e3. PMID: 28772124

15. Nakamura NH, Flasbeck V, Maingret N, Kitsukawa T, Sauvage MM. Proximodistal segregation of nonspatial information in CA3: preferential recruitment of a proximal CA3-distal CA1 network in nonspatial recognition memory. J Neurosci Off J Soc Neurosci. 2013 Jul 10;33(28):11506–11514. PMCID: PMC6618684

16. Hunsaker MR, Kesner RP. Dissociations across the dorsal-ventral axis of CA3 and CA1 for encoding and retrieval of contextual and auditory-cued fear. Neurobiol Learn Mem. 2008 Jan;89(1):61–69. PMCID: PMC2675280

17. Hunsaker MR, Rosenberg JS, Kesner RP. The role of the dentate gyrus, CA3a,b, and CA3c for detecting spatial and environmental novelty. Hippocampus. 2008;18(10):1064–1073. PMID: 18651615

18. Conrad CD, Ortiz JB, Judd JM. Chronic stress and hippocampal dendritic complexity: Methodological and functional considerations. Physiol Behav. 2017 Sep 1;178:66–81. PMID: 27887995

19. Hunt DL, Linaro D, Si B, Romani S, Spruston N. A novel pyramidal cell type promotes sharp-wave synchronization in the hippocampus. Nat Neurosci. Nature Publishing Group; 2018 Jul;21(7):985–995.

20. Sun Q, Jiang YQ, Lu MC. Topographic heterogeneity of intrinsic excitability in mouse hippocampal CA3 pyramidal neurons. J Neurophysiol. 2020 Oct 1;124(4):1270–1284. PMCID: PMC7717164

21. Holley ZL, Bland KM, Casey ZO, Handwerk CJ, Vidal GS. Cross-Regional Gradient of Dendritic Morphology in Isochronically-Sourced Mouse Supragranular Pyramidal Neurons. Front Neuroanat [Internet]. 2018 [cited 2022 Aug 9];12. Available from: https://www.frontiersin.org/articles/10.3389/fnana.2018.00103

22. Swinehart BD, Bland KM, Holley ZL, Lopuch AJ, Casey ZO, Handwerk CJ, Vidal GS. Integrin β3 organizes dendritic complexity of cerebral cortical pyramidal neurons along a tangential gradient. Mol Brain. BioMed Central; 2020 Dec;13(1):1–15.

23. Feng G, Mellor RH, Bernstein M, Keller-Peck C, Nguyen QT, Wallace M, Nerbonne JM, Lichtman JW, Sanes JR. Imaging neuronal subsets in transgenic mice expressing multiple spectral variants of GFP. Neuron. 2000 Oct;28(1):41–51. PMID: 11086982

24. Malik R, Dougherty KA, Parikh K, Byrne C, Johnston D. Mapping the electrophysiological and morphological properties of CA1 pyramidal neurons along the longitudinal hippocampal axis: DORSOVENTRAL GRADIENT IN EXCITABILITY OF CA1 NEURONS. Hippocampus. 2016 Mar;26(3):341–361. PMCID: PMC4760884

25. Gaarskjaer FB. Organization of the mossy fiber system of the rat studied in extended hippocampi. I. Terminal area related to number of granule and pyramidal cells. J Comp Neurol. 1978 Mar 1;178(1):49–72. PMID: 632370

26. Schindelin J, Arganda-Carreras I, Frise E, Kaynig V, Longair M, Pietzsch T, Preibisch S, Rueden C, Saalfeld S, Schmid B, Tinevez JY, White DJ, Hartenstein V, Eliceiri K, Tomancak P, Cardona A. Fiji: an open-source platform for biological-image analysis. Nat Methods. Nature Publishing Group; 2012 Jul;9(7):676–682.

27. Lein ES, Callaway EM, Albright TD, Gage FH. Redefining the boundaries of the hippocampal CA2 subfield in the mouse using gene expression and 3-dimensional reconstruction. J Comp Neurol. 2005 Apr 25;485(1):1–10.

28. Zhao X, Lein ES, He A, Smith SC, Aston C, Gage FH. Transcriptional profiling reveals strict boundaries between hippocampal subregions. J Comp Neurol. 2001 Dec 17;441(3):187–196.

29. San Antonio A, Liban K, Ikrar T, Tsyganovskiy E, Xu X. Distinct physiological and developmental properties of hippocampal CA2 subfield revealed by using anti-Purkinje cell protein 4 (PCP4) immunostaining. J Comp Neurol. 2014 Apr 15;522(6):1333–1354.

30. Lorente De Nó R. Studies on the structure of the cerebral cortex. II. Continuation of the study of the ammonic system. J Für Psychol Neurol. 1934;46:113–177.

31. Feng L, Zhao T, Kim J. neuTube 1.0: A New Design for Efficient Neuron Reconstruction Software Based on the SWC Format. eNeuro [Internet]. Society for Neuroscience; 2015 Jan 1 [cited 2022 Aug 4];2(1). Available from: https://www.eneuro.org/content/2/1/ENEURO.0049-14.2014 PMID: 26464967

32. Longair MH, Baker DA, Armstrong JD. Simple Neurite Tracer: open source software for reconstruction, visualization and analysis of neuronal processes. Bioinforma Oxf Engl. 2011 Sep 1;27(17):2453–2454. PMID: 21727141

33. Akram MA, Nanda S, Maraver P, Armañanzas R, Ascoli GA. An open repository for single-cell reconstructions of the brain forest. Sci Data. 2018 Feb 27;5:180006. PMCID: PMC5827689

34. Ascoli GA, Donohue DE, Halavi M. NeuroMorpho.Org: a central resource for neuronal morphologies. J Neurosci Off J Soc Neurosci. 2007 Aug 29;27(35):9247–9251. PMCID: PMC6673130

35. Scorcioni R, Polavaram S, Ascoli GA. L-Measure: a web-accessible tool for the analysis, comparison and search of digital reconstructions of neuronal morphologies. Nat Protoc. 2008;3(5):866–876. PMCID: PMC4340709

36. Benjamini Y, Krieger AM, Yekutieli D. Adaptive linear step-up procedures that control the false discovery rate. Biometrika. 2006 Sep 1;93(3):491–507.

37. Yu Z, Guindani M, Grieco SF, Chen L, Holmes TC, Xu X. Beyond t test and ANOVA: applications of mixed-effects models for more rigorous statistical analysis in neuroscience research. Neuron. 2022 Jan;110(1):21–35.